A. Scientific Background

Biological Molecular Motors: Biological molecular motors made of proteins, which play major roles in many biological processes, often operate with remarkably high chemical yield and speed. Bipedal walkers such as kinesin can perform hundreds of steps at a rate of hundreds of steps per second before dissociating from the microtubule track, and rotary motors such as F1-ATPase and bacterial flagellum can rotate at rates of ten to thousands of rotations per seconds and up to a million times before they cease to operate[1-6] (Fig. 1). These molecular motors have several notable characteristics: (i) By consuming energy they progress directionally or bidirectionally[3] and, therefore, can perform work (i.e., they are not governed only by Brownian motion). (ii) As in the case of enzymes, there is no irreversible chemical change to these biological motors themselves during operation (no "burnt-bridge" mechanism[7-8]), and, as a result, there is in principle no limitation on the number of operations they can execute. (iii) Biological motors typically perform many repeated operation before dissociating or halting operation for other reasons (defined as processivity[1]). Finally, (iv) biological motors are autonomous, meaning, given the right set of conditions (e.g., an energy source) they do not require external intervention to function. Biological motors are typically very energetically efficient; however, this property is beyond the scope of the current proposal and will not be discussed further. Inspired by biological machines, many synthetic molecular machines and devices made of various types of molecules and that have some of the characteristics of biological motors have been demonstrated [9-16]. To date, however, no molecular motor that is directional, does not undergo irreversible chemical change, is processive, and is autonomous has been demonstrated, with the exception of one recent example[17].

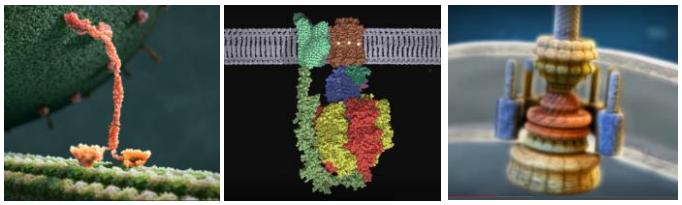

Fig. 1: Illustrations of Biological Motors. From left to right: bipedal kinesin, F1-ATPase, and bacterial flagellum rotary motors. Biological rotary motors are typically much more processive than bipedal walkers.

Challenges for Synthetic Molecular Motors: To fabricate molecular motors with characteristics of biological motors, and even with much lower operation rates and processivity, some very demanding engineering and synthetic challenges have to be addressed. First, we will have to engineer and assemble a molecular complex with well-designed and specific structure and topology that will constitute the motor scaffold. This scaffold will have to be structurally robust, yet flexible in designed locations. Even more demanding, a propulsion mechanism that can power the motor will have to be designed and properly integrated into the motor molecular complex; here we focus only on mechanisms that are based on chemical reactions, but light-, electric- and magnetic-based mechanisms are also possible[18-21]. Likely the most difficult task, some kind of motor internal coordination mechanism must be developed. For example, for the bipedal kinesin walker to avoid dissociation from the microtubule track, the trailing leg must somehow 'know' not to detach from the track before the leading leg is stably anchored[22]. Dissociation is less of a problem for biological rotary motors than for biological bipedal walkers, because the rotors are partially or fully encased

inside the main body frames (in addition to stabilization by the cell membrane), and, therefore, a failure in coordination will typically result in temporary halt of rotation and not motor dissociation. We will use this strategy for our proposed rotary motor.

DNA Nanotechnology Tool Box: Fortunately, DNA nanotechnology may offer a set of solutions to meet most of the challenges described above[23-25], if not all[26-27]. The information encoded in the DNA molecule in the form of nucleotide sequence dictates DNA interaction strengths and hierarchies, and, as a result, DNA molecules can be assembled into programmable, predictable, and well-defined structures[28-29]. The DNA origami technique allows the assembly of robust two- and three-dimensional structures, typically several dozen nanometers in size[30-32], and larger and more complex structure can be assembled by joining origami building blocks together[33-38]. Such origami structures can serve as the main structural element of molecular motors, to which, the energy providing machinery can be integrated[38-45]. Furthermore, single-stranded DNA hybridization reactions can provide energy for powering molecular motors[26-27, 38, 42, 44, 46-55] and can provide programmable structural flexibility where needed[56-60].

Passive Rotary Device Made of DNA: An illustrative example, directly relevant to our proposal, of how molecular motors can be fabricated using DNA is presented in Fig. 2. Dietz and coworker[61] fabricated a passive rotary device from three multilayer DNA origami[31-32] building blocks. A rotor element was encased inside a cavity consisting of two clamp units with assembly assisted by 'socket' elements[37]. Tightening two bracket elements resulted in irreversible trapping of the rotor inside the clamps, solving the challenge of processivity for this rotary device. Using single-particle tracking fluorescence microscopy the authors showed that, excluding transient docking of the rotors by the socket elements, the rotor freely rotates inside the cavity (Brownian rotation), often faster than the experimental time resolution (50 ms). These results are very encouraging because they demonstrate that a rotor can be locked inside a cavity while maintaining free rotation. This passive rotary apparatus lacks an energy-driven propulsion mechanism. To develop an active rotary motor, a propulsion mechanism will have to be developed and integrated into a modified device.

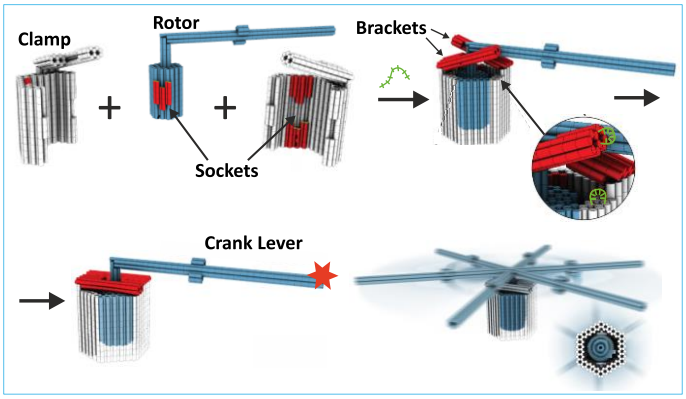

Fig. 2: Passive rotary device made of DNA. Illustration adapted from ref. Assembly of the clamps and the rotor was assisted by shape-complementary sockets. Two bracket elements locked the rotor inside the cavity by hybridization of auxiliary strands (green). Because of socket interaction some rotors transiently docked. When not docking, the rotor rotates on the tens of milliseconds time scale. The position of a fluorophore (red star) attached on the tip of a long crank lever (1 μm or shorter) reported the rotor orientation.

DNA Motors with Autonomous Propulsion Mechanisms: Several DNA autonomous motor designs have achieved directionality[7, 39-41, 49, 51] and coordination between the legs[52] (the latter was also studied by our group using single-molecule fluorescence[54]). However, directionality of these motors has been achieved only by irreversibly damaging the track on which the walkers stride, and, therefore, the motors operate only once.

Turberfield and coworkers designed a bipedal motor that, at least in principle, is autonomous, directional, and free of bridge burning[26-27]. This was achieved by smart coordination between the legs (as well as other tricks); however, only two steps were demonstrated. To the best of our knowledge, there is no published working plan for how to achieve an autonomous, directional, processive, and non-burning bridge motor made of DNA. The externally controlled rotary motor that we propose here will be instrumental step toward future realization of such autonomous rotary motor.

Externally Controlled Propulsion Mechanisms: Adopting a different strategy for DNA motors, researchers intentionally sacrifice autonomy in favor of directionality, avoiding the burnt bridge effect, and enabling coordination (i.e., between legs) and processivity. In this approach, an externally introduced DNA strand, called 'Fuel', joins two other strands together[46] (e.g., a walker's leg and a corresponding foothold). Consecutive introduction of 'antifuel' strands, which have sequence complementary to that of the fuel, removes the fuel via a toehold-mediated strand displacement reaction process[46]. Using this mechanism DNA bipedal walkers have been driven to walk on an asymmetrical DNA track with inchworm[47] and hand-over-hand[48] gaits with 2 and 5 precise and controlled steps and movement over ~7 and ~25 nanometers, respectively. These bipedal motors, which are powered by sequential hybridization of fuel and antifuel strands, are directional (in fact, controllably bidirectional) and do not undergo irreversible chemical changes.

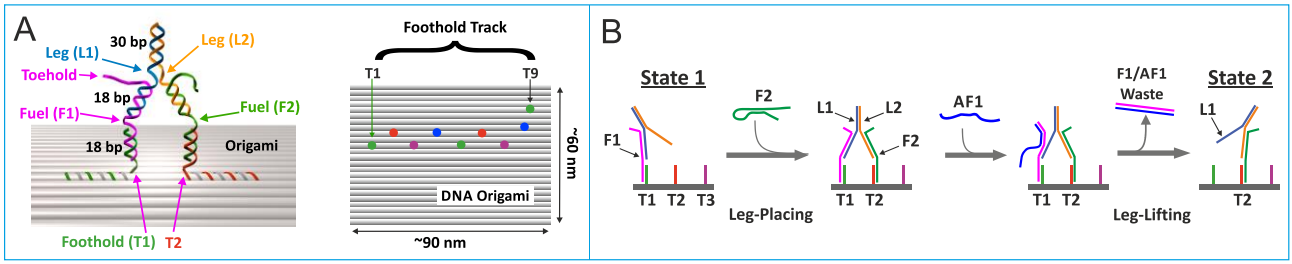

Fig. 3: Bipedal motor design and operation mechanism. (A) The bipedal motor consists of a two leg walker (L1 and L2) and ten foothold strands track (T1-T9, different colors indicate different DNA sequences) imbedded in rectangle DNA origami. Each of the two legs can connect to the footholds via two fuel strands (i.e., F1 and F2). (B) Principle of motor operation: walking from state 1 to state 2. Fuels have four possible sequences (F1-F4) and four antifuels have complimentary sequences (AF1-AF4). External introduction of F2 results in attachment of L2 to T2. Introduction of AF1 removes F1 through a toehold mediated strand displacement reaction (ref), results in lifting of L1 and generating a waste product (F1/AF1 duplex) and arrival of the motor to state 2. Sequential introduction of the four fuel and antifuels strands results in directional movement along the asymmetrical track without irreversibly changing the walker or the track.

To enable a larger number of steps, our group embedded the footholds of the hand-over-hand-type bipedal motor in a structurally robust 90-nm long rectangle origami asymmetrical track (Fig. 3) and demonstrated its operation using single-molecule FRET[44]. We have also showed that the bipedal walker can stride back and forth between two origami units joined together[38]. Most important for this proposal, our studies revealed two major fundamental problems that substantially limit motor performance: accumulation of redundant strands and the formation of trapped state. The first can be solved by the usage of microfluidics device and the second is addressed in this proposal.

Accumulation of Redundant Strands and Our Microfluidics-Based Solution: One major problem for externally controlled motors is the accumulation of redundant fuels and antifuels in the solution. To solve this problem, possibly in its entirety, we developed a microfluidics[62-63] that enables delivery of fuel and antifuel strands to molecular motors that are immobilized on a glass coverslide inside the microfluidics device and removal of redundant and used fuel and antifuel strands from the solution (Fig. 4A, this work has been submitted to *Nano Letters*). The microfluidics device is mounted on a single-molecule total internal reflection optical setup (smTIRF[64-65]) that allows real-time monitoring of the walker's progress. With this operation scheme, our origami-based bipedal motors performed 32 steps (total of 64 leg-lifting and leg-placing reactions) with 44% total operational yield (defined as the percentage of motors that operated as intended) transiting 370 nanometers, including three externally controlled turns in the walking direction (Fig, 4B). In comparison, an identical motor that was operated free in solution without removal of fuel and antifuel strands, performed only five to six steps with a total yield of 44% (Fig. 4C). During operation of the unwashed motor, redundant out-of-phase antifuels detached the walker from the track, and fuels ordered the bipedal motor to walk in the wrong direction[44]. These artifacts were not observed for the microfluidics-driven motors (e.g., no incorrect populations were observed in the FRET histograms, Fig. 4B). To the best of our knowledge, the number of steps achieved with this microfluidics-driven motor is the highest for any externally controlled DNA molecular motor or other DNA device to date. That the motor perform only 32 steps (2.5% walker dissociate at each step) is the trap-state problem as we explain below and address with this proposal.

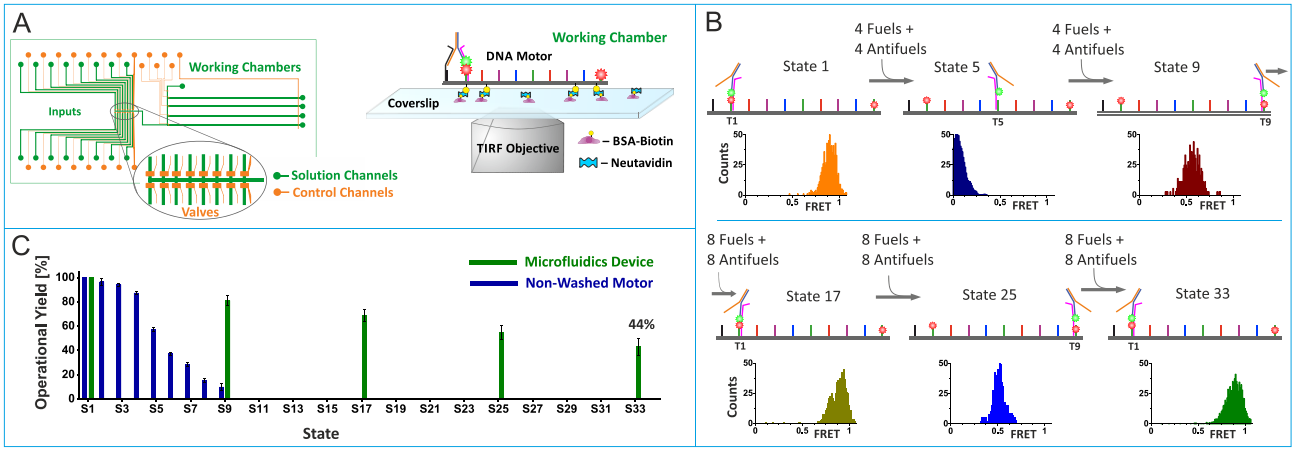

Fig. 4: Microfluidics and single-molecule experimental setup and 32 steps performed by origami-based bipedal motor. (A) Microfluidics device: Input channels (green) feed the 'working chambers' and are controlled by a set of imbedded valves (pneumatics pressure provided by 'control channels', orange). The device is mounted on a TIRF setup, and the motor is immobilized (through biotin-NeutrAvidin interactions) inside the working chamber. (B) The microfluidics conveyed a sequence of 32 fuel and 32 antifuel strands, and the motor proceeded from state S1 to state S33. Six selected states and the corresponding single-molecule FRET histograms are shown. FRET measurements were based on donor fluorophore (green star) labeled on L1 and two acceptor fluorophores (red stars) labeled on T1 and T9 at different distances from the origami. (C) The bipedal motor operated by microfluidics performed 6 fold more operations than an identical non-washed motor.

The Trap-State Effect:

Processivity: The second major problem occurs due to binding of two fuels (of the same sequence), one to the leg and the other to the foothold; for correct operation one fuel strand should connect the leg and the foothold (Fig. 5A). This undesired mechanism, (called 'trap state effect'), prevents the attachment of the leg to the foothold and lead to walker dissociation upon the introduction of the consecutive antifuel. We have shown previously that the trap state effect can be mitigated by using fuels that contain a hairpin structure[44]. These fuels are designed to first bind the foothold followed by opening of the hairpin loop and, subsequently, binding to the leg. As our microfluidics-based measurements of the motor operational yield dependency on fuel hairpin concentration and the very good agreement with a trap-state kinetic model of operational yield show, use of hairpin fuels does not entirely solve the trap-state problem and especially not in high fuel (hairpin) concentrations (Fig. 5B). Moreover, the trap-state mechanism places significant limitations on the motor's speed.

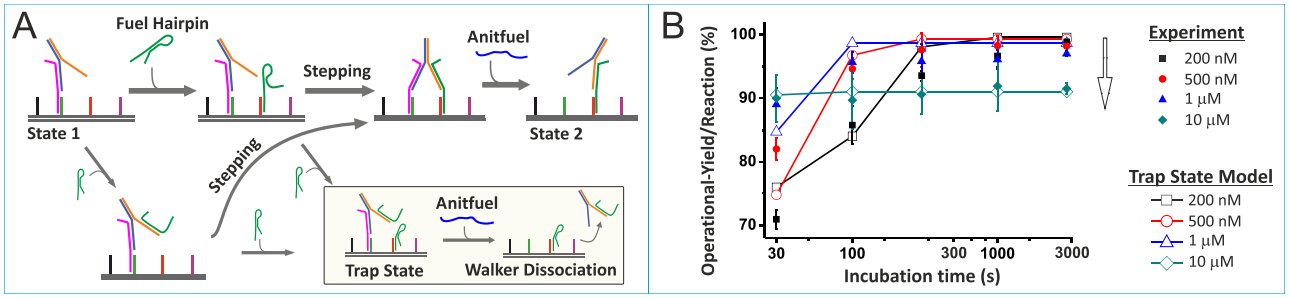

Fig. 5: The Trap state effect. (A) The 'trap-state' model: A hairpin fuel is designed to bind the foothold and then open and bind the leg. However, another fuel may bind the leg before the leg and the foothold associate, leading to the formation of a stable 'trap state' and walker dissociation upon the addition of consecutive antifuel. (B) Experimental and simulated operational yields at different fuel and antifuel concentrations and incubation times. Increased fuel concentration decreased the yield (gray arrow). The very good agreement between the experimental resulsts and the calculated trap-state kinetic model operational yields indicates that the trap state is the main reason for motor dissociation.

Motor speed: The velocity of externally controlled motors depends on the rate at which consecutive fuel and antifuel commands are provided to the motor. Faster rates (i.e., shorter incubation times) enable faster motor operation. However, motors that do not react in the given incubation time will dissociate in the consecutive step. Thus, motor processivity and speed are interlinked. We have measure the leg lifting rate and the leg placing rate using the microfluidics fast solution exchange rate (0.07 seconds for the imaged area, Fig. 12A). ***Leg lifting:*** We found that the leg lifting rate is linearly dependent on antifuel concentration ($k_{LL} = 2.4 \times 10^5 M^{-1}s^{-1}$) and that given sufficient time and antifuel concentration, 100% (measurement error: ~1%) of the legs were lifted (Fig. 12B and ref[44]). Base on this rate, 10 µM antifuels should result in 99.9% leg lifting in 3 seconds. Therefore, the leg lifting reaction does not place significant limitations on motor processivity or speed. ***Leg placing:*** Fitting of the leg placing results yielded the fuel binding rate and the bipedal steeping rate (Fig. 12C). The stepping rate, which is the time it takes the leg to associate with the foothold after a fuel strand binds (an intra-molecular reaction), is $k_S = 0.135\ s^{-1}$. Accordingly, without the trap-state effect, this reaction can achieve 99.9% stepping in 50 seconds. However, for 99.9% of the motors to bind fuels in 50 seconds, the fuel concentration must be higher than 2.3 µM ($k_{FB} = 0.64 \times 10^5 M^{-1}S^{-1}$, Fig. 12C), and according to our measurements and model (Fig. 5), this concentration results in ~3% trap-state per step.

Therefore, the motor yield and speed are both limited by the trap-state effect. It should be noted that the problem described here is arguably relevant to any externally controlled DNA motor or device that operates using fuels that bind two other strands (e.g., legs and footholds). Therefore, addressing the trap-state problem is essential for achieving fast and processive externally controlled motors and other devices.

B. Research Objectives and Expected Significance

Goals and Specific Aims: Realization of bioinspired molecular machines that consume energy and perform work is a complex task. To the best of our knowledge there is no published proposal that suggests a rational path towards the realization of autonomous, processive, and directional DNA motors that do not burn the bridge. The long-term goal of our research is to develop both externally controlled and autonomous processive and fast motors. Because autonomous function is significantly more complicated than external control, we strategically choose to focus first on the development of externally controlled motors. Using a microfluidics device, my group has solved the problem of the accumulation of redundant energy-providing and commanding DNA strands, a necessary step toward the realization of motors that respond to a large number of commands. The second major problem is the trap state, which reduces processivity and speed. We will deal with this problem here. Our efforts will have benefits for externally controlled motors and other externally controlled devices, will further our understanding of complex DNA dynamics, and, finally, will place us in a position that will allow the development of autonomous rotary motors as we explain below.

The specific goal of this proposal is to develop externally controlled DNA-based molecular motors that are capable of performing hundreds to thousands of operations with high yield and speed. Relying on our extended understanding of the mechanisms that operate in externally controlled DNA motors, our development of microfluidics technology for delivering and removing operating strands, single-molecule spectroscopy for monitoring motor operation, and recent advances in multilayered DNA origami technology, we will develop a new strategy for processive and fast bipedal linear motors (Aim 1) and a novel highly processive and fast rotary motor (Aim 2).

Aim 1. Develop a strategy for fast and efficient operation of externally controlled motors and demonstrate hundreds of steps with high operation rate: We will develop a new and significantly improved strategy for the operation of bipedal motors that completely avoids the harmful trap-state effect. The strategy is based on reversing the order of fuels and antifuels provided to the motor (called 'fuel before antifuel' or FBAF). First, a fuel is placed on the foothold before the corresponding leg is lifted and the redundant strands are washed away. Then, the consecutive antifuels are introduced, lifting the corresponding leg that then binds the fuel on the corresponding foothold and the motor moves forward. Because redundant fuels are absent from the solution the leg can bind only the correct fuel. For this strategy to avoid unwanted interactions between fuels and the consecutive antifuels, the antifuel strands will be shortened and fuel and antifuel redesigned accordingly. With this strategy, increased concentrations of fuels and antifuels will accelerate leg placing and leg lifting reactions without negative effect on reaction yield. The only limitation on motor speed will be the intrinsic intramolecular stepping reaction. Based on our measurements of the kinetics of the reactions involved in our original bipedal motor (Fig. 3-5 and 12-13, submitted to *Nano*

Letters), we expect that two orders of magnitude improvement in processivity and speed are in reach. Hundreds, and possibly thousands, of steps with about one minute per step should be possible. The motor will be operated and characterized using microfluidics and single-molecule FRET-TIRF as we did previously for our bipedal motor (Fig. 4). The microfluidics device is computer controlled and very reliable and can deliver many thousands of commands without errors[62-63]. Single molecule measurements will be conducted in different locations in the working chamber (Fig. 4A); therefore, bleaching does not constitute an obstacle.

Aim 2. Develop a robust rotary motor that is free from the problem of processivity: We will develop an externally controlled rotary motor in which a multilayer origami rotor is encapsulated inside a multilayer origami frame. The rotor and the frame will be attached by a single-stranded DNA swivel element that will allow free rotation but prevent dissociation of the rotor from the frame in the event of error in operation. The motor will be powered by two or more bipedal motors (refined in Aim 1). Unlike the linear motor, the rotary motor will not dissociate. This will allow higher frequency of fuel and antifuel introductions and, therefore, more steps per minute. The motor operation will be monitored by analysis of the polarization of light scattered from a single gold nanorod attached to the rotor head. The high resolution of the light scattering technique and the fact that the rotary motors will remain intact will allow much more detailed study and optimization of the motor than is possible for the linear bipedal motor, and this can assists in future development of autonomous rotary motor.

Expected Significance: Despite many efforts, autonomous or externally controlled motors or other DNA machines and devices that can perform many precise operations have not yet been demonstrated. ***Our plan to develop such a motor has the potential to change the perception about what is possible in terms of rational design, synthesis, assembly, and, particularly, operation, of molecular motors and other devices***, facilitating many developments. Directly related is the realization of autonomous motors: One of the goals of nanotechnology, and DNA nanotechnology in particular, is the development of autonomous motors. By replacing the externally controlled propulsion mechanism with autonomous mechanism, for example, like the one demonstrated by Turberfield and his coworkers[26-27], the rotary device proposed here can, potentially, operate autonomously. Avoiding the problem of rotor dissociation and using the high resolution of the light scattering method will significantly promote such development. Such a motor will not require the external introduction of strands for normal operation; however, the microfluidics can be very instrumental in the development phase. ***The proposed work has implications for design of other DNA-based devices.*** The operation mechanisms proposed here and insights into motor dynamics and the microfluidics strategy should be useful for the development of user-controlled precise DNA devices in addition to motors. This includes DNA assembly lines for the synthesis of other molecules[42, 66], DNA mechanical components such as crank-slider[56] and rotaxane[67], mechanical manipulators of host molecules[68-69], and semi-autonomous DNA computing devices[70-72]. Functions such as externally commanded peaking and placing of cargo is essentially the same challenge as connecting and disconnecting legs to footholds, and success with our operation mechanism and the microfluidics strategy will enable development of devices with many orthogonal operations. ***There are benefits in studying a repeatable machine:*** A major advantage of studying molecular

machines that perform many repeated operations is that it allows recognizing, studying, and potentially resolving even minor flaws in the machine. For example, an operational flaw that reduces the yield by an undetectable 1% per step would reduce the total yield by more than 20% after 23 steps. These flaws may include chemically truncated strands, transient undesired weaving of strands into the origami, and others. The information acquired in the study we propose, therefore, will be relevant to broad range of DNA nanotechnology applications. ***Finally, our work will shed light on DNA dynamics and interaction.*** As we demonstrated in our study of our original bipedal motor, necessities related to the improvement of the operational mechanism encourage detailed study of DNA dynamics and interaction, including complex reaction cascades in context of three dimension architecture and in the vicinity of origami structures.

C. Research Design, Methods, Hypothesis and Preliminary Results

Aim 1. Develop a strategy for fast and efficient operation of externally controlled motors and demonstrate hundreds of steps with high operation rate:

Linear motor – principles of fuel before antifuel strategy: The fuel before antifuel strategy (FBAF) is designed to completely avoid the trap state effect. A high concentration of fuels (i.e., F3; Fig. 6) will be introduced when the corresponding leg (L1) is still placed on foothold (T1). The fuel will quickly bind the footholds (e.g., 30 µM should achieved 99.9% yield in 4 s, $k_{FB} = 0.64 \times 10^5 M^{-1} S^{-1}$; Fig 12C). The fuel will not bind to L1 because L1 is attached to F1. Then, the redundant fuels will be removed by thoroughly washing using the microfluidics. Antifuel strands (AF1) will then be introduced at high concentration, resulting in rapid lifting of L1 (e.g., 10 µM should achieve 99.9% leg lifting in 0.4 s, $k_{LL} = 2.4 \times 10^5 M^{-1} S^{-1}$; Fig 12B). The F3 segment that binds the leg is complementary to AF1 (this is unavoidable). To avoid irreversible binding of AF1 to F3 (which will prevent the completion of the leg-placing reaction), we will shorten the antifuels by nine bases such that the AF1/F3 duplex is only nine base pairs long (the leg is 18 bases). It was shown previously[73] that a 9-bp duplex, one side attached to origami, thermally dissociates at a rate of $k_{Diss} = 1.6\ s^{-1}$. Accordingly, 99.9% of the duplexes are expected to dissociate within 5 s upon microfluidics-based removal of the redundant antifuels (which prevents re-association of AF1 to F3). Because the antifuels will be shortened, F1 will not be completely removed from L1 by AF1. However, the 9-bp F1/L1 duplex is also expected to dissociate at a rate similar to the AF1 dissociation. After the removal of AF1 and F1/AF1 duplex the steeping reaction will take place (99.9% stepping reaction in 50 s, at a rate of $k_S = 0.135\ s^{-1}$; Fig 12C). The microfluidics solution exchange time is about 0.1 s (Fig. 12A). Therefore, we expect ~100% washing of fuels and antifuels within 1 second, as will be tested by monitoring the motor performance under different washing conditions.

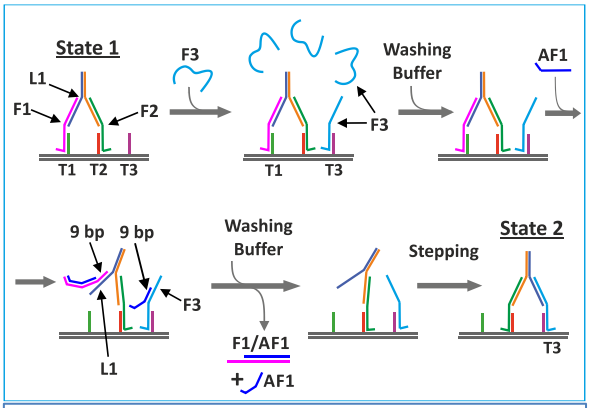

Fig. 6: Fuel before antifuel strategy (FBAF).

Expected performance: Assuming these reaction times and yields, the motor will be able to perform 100 steps (total of 1500 nm) with 50% total yield within about 60 minutes or with 90% total yield within about 80 minutes (longer waiting time for the stepping reaction), or 1000 steps with 90% yield within 18 hours. The 32 steps and 44% yield that were achieved using the original motor would be achieved within about 15 minutes, which is 100 times faster than the original motor (Fig. 4 and 5). Because with the FBAF strategy there are no principle limitations on fuel and antifuel concentrations (and the fuel displacement rate is very fast, Fig. 12B), the intramolecular stepping reaction is the main factor that limits performance. The calculations presented above are for fuels with hairpin structure. The unstructured fuels that we will use here are expected to hybridize the leg significantly faster than fuels with hairpin structure (possibly by a 10 fold[55]) and, therefore, are expected to increase the stepping rate and the motor performance accordingly.

Possible additional mechanisms and flaws: The calculations of the expected yields and speeds presented in this proposal are based on the assumption of homogeneity of the motors and of the fuel and antifuel strands. For example, the stepping reaction behaves according to a first-order model with a single rate constant, and the fuel and antifuel binding reactions behave according to pseudo first-order models with a single rate constant (because their concentrations are much higher than that of the motors). Although these reactions generally behave according to these basic models, as indicated by our kinetic experiments (Fig. 12), it is not unlikely that additional minor interfering mechanisms exist. For example, a small fraction of the motors occasionally assumes a metastable conformation that significantly slows the steeping reaction (e.g., a leg and a foothold pointing in different directions) or a small fraction of fuels is chemically truncated such that a fuel binds and blocks the foothold but does not bind the leg. Such hypothetical mechanisms may reduce motor performance in comparison to our calculations. We argue, however, that only by avoiding the current major cause for motor failure, the trap-state effect, we will be able to identify and potentially resolve such problems, if they exist. We describe below how by using two identical footholds tracks we will deal with the potential problem of truncated fuel strands.

Measurements of motor operation and optimization: The motor will be operated and measured using the same microfluidics and FRET-TIRF system we are using daily and that was used for the early version of the bipedal motor (Fig. 4 and 13). The motors will be immobilized on the coverslip inside the microfluidics device and provided with a sequence of fuels and antifuels and washing buffer according to the procedure described in Fig. 7. The operational yield will be measured by counting the number of motors with the proper FRET value when parked on foothold T1 or T9 (high and intermediate FRET values, respectively; Fig. 4). To avoid fluorophore bleaching, measurements will be conducted in different locations in the working chamber (Fig. 4A). Different fuel and antifuel concentrations and different incubation and washing durations will be examined and optimized in terms of operational yield and speed. The dependency of operational yield on these parameters will provide information on the reaction rates and mechanism of the FBAF strategy. Depending on results obtained, we may optimize the lengths of the antifuels, fuels, legs, and footholds. We will also evaluate unpurified, purified, and double purified fuels.

Preliminary results: Our preliminary results are very promising. We have measured the yield of a leg placing reaction at 10 µM fuels concentration with the FBAF strategy and found that ~100% of the legs were placed correctly on the foothold after 5 minutes as expected from FBAF strategy (Fig. 7A). Under the same conditions, the motor operated with the original method showed 35% dissociation. The error of the measurement was about 1% (10000 individual motors were counted). This measurement was of only one leg placing reaction (repeated several time to increase statistics), not from a motor walking repeatedly along a track. We will test and optimize the FBAF strategy over multiple steps and command the walker to walk back and forth over the full-track length, as we did for the original motor (Fig. 4).

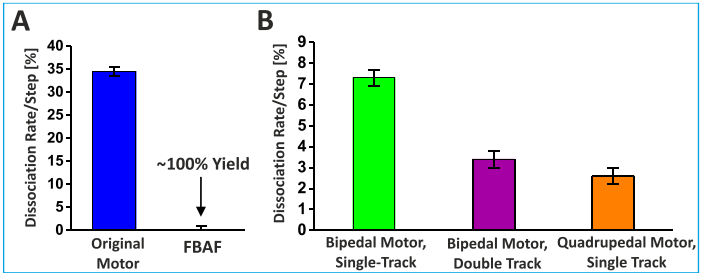

Fig. 7: (A) Preliminary results for FBAF: About one hundred precent of the legs were correctly placed on the foothold using the FBAF stratagy in conditions in which the original method show 35% dissociation dew to the trap state effect. (B) Double track motors shows 2 fold decrease in dissociation rate in respcet to single track motors. Quadruprdal walker shows 2.5 fold decrease in dissociation in respect to bipedal walker. The dissociation rates were intentially increased by usage of high fuel and fuel hairpin concentrations (10 µM, A and B, respectivly).

Double track motor and its benefits: To further increase motor processivity and motor speed for a given processivity we will double the number of footholds. We will prepare the origami with two sets of footholds to form two identical parallel tracks 5 nm apart. Doubling the number of footholds will allow two identical fuels to bind the track simultaneously, and this has two major benefits: (i) Assuming the absence of steric interference between the two fuels, binding will occur to the leg (stepping reaction) at twice the rate of a single foothold, and this should double the yield and speed of the motor. Our measurements of the original motor (not using the FBAF strategy) showed about 2-fold increase in processivity for the double-track motors compared to single-track motors, as expected (Fig. 7B). (ii) In the case in which a foothold is unavailable, for example, because it has transiently weaved into the origami or in the case of a chemically truncated fuel (although fuels will be PAGE purified, as all the other important strands) binds one of the footholds the other identical foothold-fuel complex will likely be available for interaction with the leg. We have no evidence that foothold weaving takes place or that a significant fraction of fuels are truncated, but we cannot exclude these two effects entirely. Because the probability that two foothold-fuel complexes will not be available at the same time is very low (a product of two low probabilities), the double track approach should reduce these effects approximately exponentially. We also analyzed a quadrupedal walker walking on a single track and found a 2.5-fold increase in processivity relative to bipedal motor (Fig. 7B).

Upon achieving bipedal motors that can perform a satisfying number of steps at satisfying rate we will be in position to demonstrate long distance walking, orthogonal operation of motors and cargo picking, maneuvering and placing. The rectangle origami track can be replaced with long origami rods which we will join together (as we did before for rectangle origami ref). This will enable demonstrating controlled bidirectional movement along hundreds of nanometers. In a different system, two motors with entirely different legs, fuels, antifuels and foothold sequences can be design to walk orthogonally on the same origami platform. DNA cargo picking and placing is essentially the same task as lifting and placing legs, therefore, the FBAF mechanism can be apply for these operations. A modified walker can pick a DNA cargo, maneuver and place it in another position.

Aim 2. Develop a robust rotary motor that is free from the problem of processivity:

General description of the rotary motor: A scheme of a conceptual rotary motor and its operation principle is presented in Fig. 8. The motor consists of two main parts, a rotor and a frame (honeycomb-type lattice origami[31-32]). The rotor consists of a cylindrical rod (called a rotor rod, blue) that is free to rotate inside the frame, and a planar rotor head. The cylindrical frame (gray), houses the rotor rod and function as a stator, and the frame is decorated with biotin molecules to allow immobilization to the coverslip (inside the microfluidics working-chamber) via an interaction with avidin on the coverslip. A key element is the swivel (purple), which is designed to lock the rotor inside the frame cavity. By rotating around its ssDNA sections, the swivel allows free rotation of the rotor inside the frame. The footholds and the legs that constitute the propulsion apparatus are embedded in the upper side of the frame stator and the bottom side of the rotor head. In addition, a gold nanorod (yellow), that will enable determination of the rotor angle using scattered polarized light, is attached to the upper side of the rotor head.

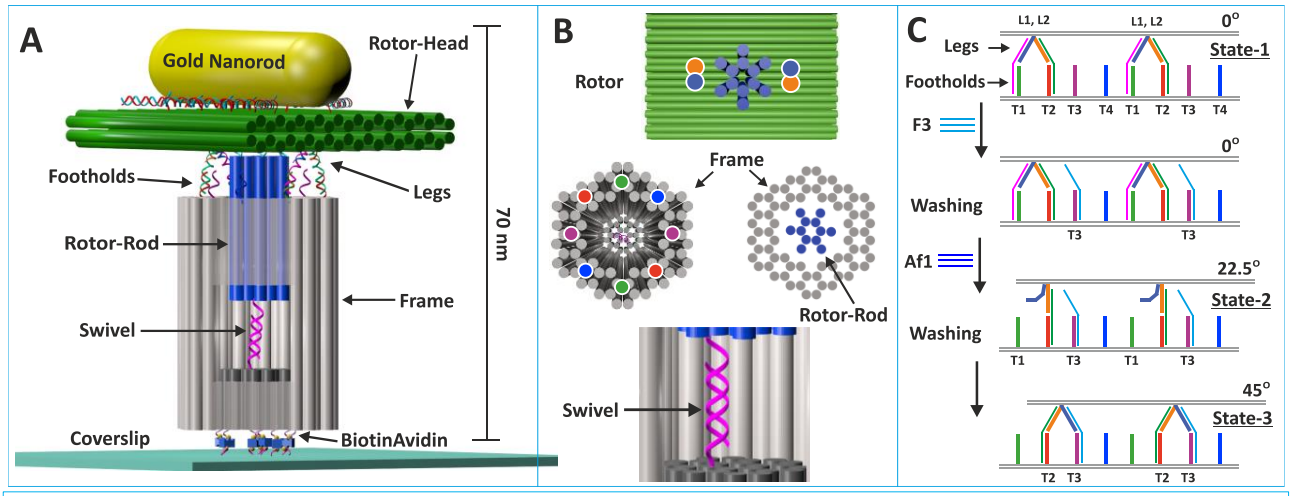

Fig. 8: (A) Illustration of the rotary motor immobilized on glass coverslip. (B) Rotor, frame, and close-up of the swivel (upper, middle, and bottom, respectively). (C) Propulsion mechanism. Only four states are shown.

Operation principle: The rotary motor can be powered using several different propulsion mechanisms. Figure 8B and C shows an extension of the FBAF mechanism to be developed in Aim 1 (Fig. 6). Four legs will be positioned on the bottom side of the rotor head at equal distances from the motor's central axis and arranged in two leg pairs (L1 and L2). Similarly, two sets of footholds T1-4, will be positioned on the upper side of the frame stator. As in the FBAF, legs will be connected to footholds via fuels F1-4 and lifted by removing the fuels with antifuels AF1-4. This mechanism is similar to the FBAF except that there are two bipedal walkers. Leg lifting and leg placing result in ~22.5° averaged rotation each (a total of ~45° from state 1 to state 3, Fig. 8C). Therefore, 16 consecutive introductions (and washings) of fuels and antifuels should result in one full rotation (360°). Repetition of this procedure will result in continuous rotation in one direction and introduction of the fuels and antifuels in reverse order will result in rotation in the opposite direction. The swivel is designed to prevent dissociation of the rotor from the frame, in case of errors in the propulsion mechanism (e.g., absence of all fuels). The swivel will contain a duplex section (~25 bp) and two ssDNA sections (~5 T bases each, Fig 8B). A ssDNA strand can rotate around its phosphate bonds at room

temperature with less than 1 kcal/mol energy barrier for rotation, at least an order of magnitude less than the energy provided by the hybridization of a fuel to a leg or a foothold (~18 bp).

Assembly of the rotary motor: There are five main synthetic tasks involved in fabrication of the rotary motor: (i) preparation of the frame, (ii) preparation of the rotor, (iii) insertion of the rotor rod into the frame, (iv) attachment of the gold nanorod to the rotor head, and (v) immobilization of the complete motor on the glass coverslip inside the microfluidics device. We will optimize each of these steps separately and then use the optimized procedures to fabricate and immobilize the completed motor.

Preparation of the frame: The frame will be constructed from multilayer DNA origami (honeycomb-type lattice) using standard procedures[31, 61]. The origami will be designed with caDNAno[74] and structurally tested *in silico* using CanDo[75]. For the scaffold, we will use standard M13mp18 DNA of the desired length[76] (tilibit nanosystems). All the relevant strands (footholds, the bottom half of the swivel, biotinylated strands, and the strands that participate in pulling the rotor, see below) will be included in the annealing mixture (corresponding staples will be omitted). Post-annealing purification will be conducted using PEG precipitation[76]. The quality of the frame will be examined using transmission electron microscopy TEM[61] (origami stained with uranyl formate, images analysis with EMAN2[77] and Xmipp[78] software for particle picking and averaging), and frame aggregation will be examined using gel electrophoresis.

Preparation of the rotor: The rotor will be prepared and characterized using the methods described for the frame with some differences. The rotor consists of a planar shaped rotor head and a perpendicular rod-shaped rotor rod (Fig. 8A and B). A similar perpendicular orientation was demonstrated for a construct of a similar size by Simmel and coworkers[79] (Fig. 9A). This construct was prepared using a one-pot annealing method on a single M13mp18 DNA scaffold, and we will adapt this approach for our rotor. In addition, we will test a modified approach describe in Fig 9B. Here, the rotor rod and head will be prepared in a one-pot annealing from a single scaffold, but we will omit the 6-8 staples that connect the two sections. These staples will be introduced after the annealing and will 'weave and weld'[33, 38] the two sections together. A tunable number of bases (2-7) will be left unpaired in the gap to relax possible structural stresses. The leg strands, the upper strand of the swivel element, anchored strands, and strands to attach the gold nanorod will be included in the annealing mixture. The rotor will be examined using TEM and gel electrophoresis.

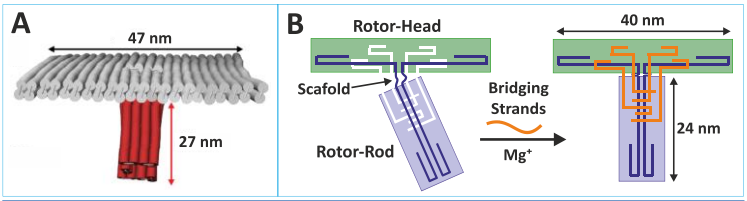

Fig. 9: (A) Illustration of the rotor designed similarly to the construct demonstrated by Simmel and coworkers (ref). (B) Alternative approach in which the staples that connect the rotor head and rod are introduced after the annealing.

Insertion of the rotor rod into the frame: Figure 10 shows a proposed mechanism to insert the rotor rod into the frame and lock the rotor and the frame using the swivel element. The frame and the rotor will be prepared separately, as described above, and then mixed at elevated Mg^{2+} concentrations. The pulling and the elongation strands are designed to bulge from the frame cavity such that the pulling strand can bind the anchor attached to the rotor head (only one set of anchors, pulling strand and elongation strand are shown in Fig. 10, but the frame can be prepared with three to six identical sets). Removing the elongation strands using anti-elongation strands and toehold-mediated strand displacement reactions should result in entropic collapse of the pulling strand pulling the rotor into the frame. Pinching strands may be added to assist in contracting the pulling strand and pulling of the rotor as was demonstrated recently by Castro and coworkers[80]. The close proximity between the two swivel strands should result in their hybridization. Finally, we will introduce anti-puling strands that will remove the puling strands and the pinching strands. A small window designed in the frame (smaller than shown in Fig. 8) will allow strands to diffuse in and out of the cavity. By placing donor and acceptor fluorophores on the swivel strands, we will monitor the attachment of the rotor and the frame using diffusion-based single-molecule alternating-laser excitation (ALEX) and the hybridization of the two swivel strands using FRET[38, 54, 64, 81]. If required, the frame-rotor construct will be purified using gel electrophoresis and extracted from the gel using the 'Freeze N Squeeze' technique[32, 43, 82]. In case that only a small percentage of the rotors are inserted into the frame, we will decrease the diameter of the rotor rod from 12 to 6 DNA bundles. We have already constructed an initial version of the frame and found that ~8 nm sized DNA construct (Holiday junction) bind the frame swivel strand at almost the same rate as hybridization of free strands. Therefore, we are quite confident that a reasonable yield can be achieved with 6 bundle rod, if not 12. This procedure will be first optimized for rotors without the gold nanorod, followed by optimization with the complete rotor with the gold.

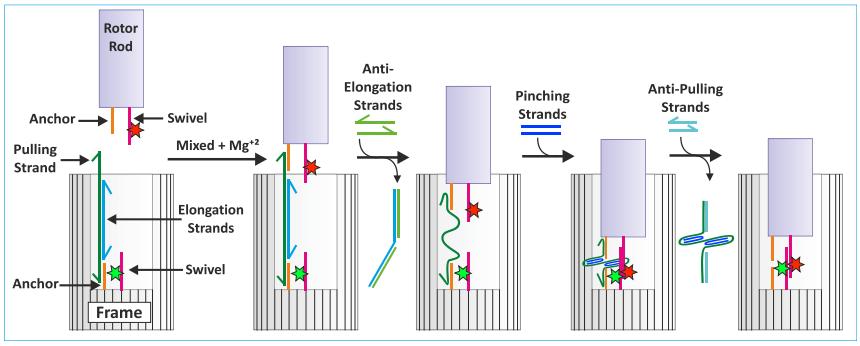

Fig. 10: Inserting the rotor to the frame. The rotor head is not shown.

Attaching the gold nanorod to the rotor head: Attaching gold nanodots and rods to origami is possible in high yields (>50-80%)[43, 83-86]. Tinnefeld and coworkers demonstrated that by using the zipper geometry (Fig, 11A) it is possible to minimize the origami-gold distance, likely reducing wiggling of the gold particle with respect to the origami. This approach allows extending the length of the attachment strands, which minimizes nanorod aggregation.[84] In short, a gold nanoroad (Nanopartz) will be functionalized with thiolated poly-T DNA strands, complementary to poly-A attached to the rotor head (elongated staples). The

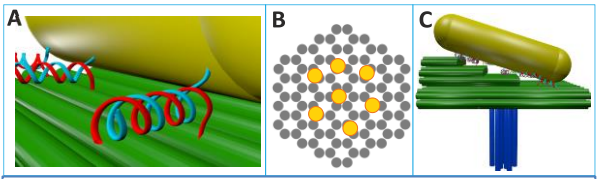

Fig. 11: (A) Attachment of the gold nanorod to the rotor head using zipper geometry. (B) Biotins will be attached only to the center of the frame base. (C) If requires, the gold nanorod will be placed at 60° relative to the main optical axis.

gold and the rotor head will be mixed at elevated temperature and left to react. The product will be purified using agarose gel and 'Freeze N Squeeze'[43]. Alternatively, non-reacting gold nanorods will be later on washed by the microfluidics[84-85]. We will use TEM imaging to verify that the gold rod is correctly positioned on the head. The procedure will be optimized on rotor head lacking the rotor rod and, after optimization, will be applied to the complete rotor.

Motor immobilization inside the microfluidics chamber: Immobilization of the motor on the glass coverslip inside the microfluidics chamber will be conducted using a method similar to that we routinely use for immobilization of the origami-based bipedal motor and other devices[64-65]. Using our method we observe almost no nonspecific immobilization (Fig. 13). In short, the plasma pretreated coverslip (before attachment to the microfluidics PDMS) will be coated with biotinylated BSA and covered with NeutrAvidin molecules (provided by the microfluidics). The base of the frame will be functionalized with 6-10 biotin molecules (modified origami staples introduced in the annealing). To minimize immobilization of the motor on its side, the biotins will be positioned in the center of the frame base (Fig. 11B). The motors will be introduced gently by the microfluidics (a slow flow) until the desired single-molecule concentration is achieved and excess motors are washed away (Fig. 13). Tinnefeld and coworkers demonstrated the immobilization of origami pillar taller than our rotary motor attached to two gold nanodots bigger than our gold nanorod[84-85]. Therefore, we expect that immobilization of the rotary motor on the coverslip will not constitute a major obstacle.

Monitoring the rotary motor operation: To monitor the rotor operation we will have to detect the rotation of the rotor with sufficient temporal and angle resolution and over long time periods. For this purpose we will implement published single-molecule methods for analysis of polarization of light scattered from the gold nanorod[5-6, 87-88]. The light scattered from a gold nanorod is about four to six orders of magnitudes stronger than the fluorescence of a typical organic dye (e.g., ATTO dyes), and gold nanorods do not blink or bleach[5]. The orientation of the rod will be determined by using the defocusing technique developed by Enderlein and coworkers[87-88]. The rotation of F1-ATPase was resolved[5-6] with these techniques with 1° azimuthal angle resolution and 10-μs temporal resolution[5]. These combined resolutions are four order of magnitude more than required for our experiments, therefore, the laser intensity (640 nm, diode laser) will be kept low (1-10 μW) to avoid radiation damage to the motor over the expected long duration of the experiment. We will use our existing camera-based TIRF setup[64-65] (in dark field mode) with only minor modifications. Data analysis for the defocusing method will be conducted using available software (provided by the Enderlein group, private discussion) with minor software modifications (Matlab or LabView, which we are familiar with) to allow real-time analysis. The method can resolve only 180° for polarization perpendicular to the main optical axis (other method resolves only 90°)[5]. If necessary to allow 360° resolution, the gold nanorod will be placed at 60° relative to the main optical axis (Fig. 11C). This may not be needed because some off-axis polarization may allow measurement of the azimuthal angle with sufficient resolution. The defocusing method can resolves 3D polarization orientation[87-88] and therefore may be able to report rotor off-axis wiggling inside the frame. Overall we expect this technique to be considerably simpler

and easier to use than the FRET-based technique we are using for the bipedal motor (higher resolution and absence of bleaching).

Characterization and optimization of the rotary motor: After immobilization of the complete motor we will characterize the motor and optimize its performance. First, we will characterize the Brownian rotation of the motor in the absence of fuels. We expect that some gold nanorods will not rotate, either because the rotary motor complex did not properly assemble or because some gold nanorods have attached nonspecifically to the coverslip surface. We will optimize the preparation and immobilization procedures to minimize the number of non-rotating signal. If needed, we will replace the 12 bundle rotor rods with six bundle rods to allow freer rotation. The motors will be attached to the coverslip in low density, such that the signals from the gold nanorod do not overlap (~50-300 motors for a camera image). Therefore, it will be possible to study the motors even if only a small percentage of the motors is active[61]. Next, we will operate the motors according to the FBAF procedure (Fig 8C) and study the motor response. The high resolution of the scattering method will allow characterization of each step and each motor state separately. Different fuels and antifuels concentrations and different incubation and washing durations will be examined, and we will examine different numbers of leg pairs and footholds. These parameters will be optimized to achieve fastest rotation rates.

Preliminary Results:

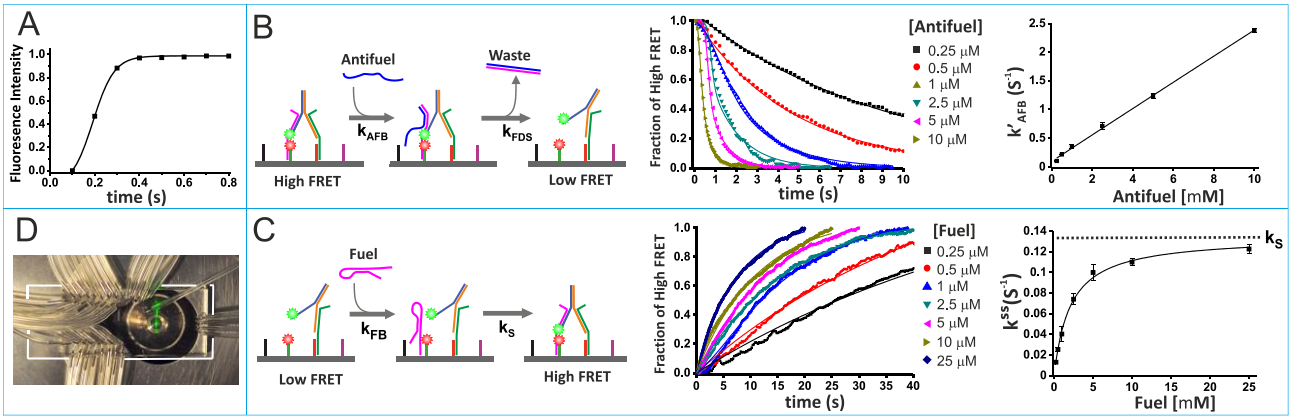

Fig. 12: Kinetic measurements. (A) Microfluidics solution exchange profile. (B) Leg lifting: Because the fuel displacement rate (k_{FDS}) is very fast (not measured here), up to a certain high concentration of antifuels, the leg lifting rate is equal to the antifuel binding rate ($k_{LL} = k_{AFB} = 2.4 \times 10^5 M^{-1}S^{-1}$). Given enough time and a high antifuel concentration, 100% of the legs are lifted. (C) Leg placing reactions: Measurements and fitting of the leg placing reactions yield the fuel binding rate ($k_{FB} = 0.64 \times 10^5 M^{-1}S^{-1}$) and the stepping rate ($k_S = 0.135\ s^{-1}$). (D) A photo of the microfluidics device placed on the TIRF setup.

Fig. 13: Immobilization of motors inside the microfluidics chamber. (A) Biotinylated BSA and NeutrAvidin are introduced. No background is detected. (B) Origami track without biotin does not immobilize. (C) Origami track with biotin does immobilize.

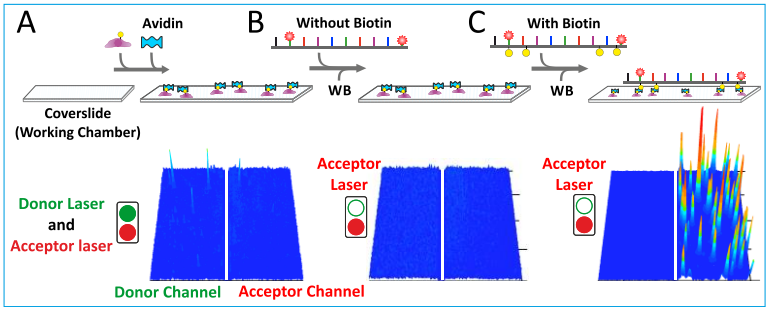

References:

1. Toprak, E.; Yildiz, A.; Hoffman, M. T.; Rosenfeld, S. S.; Selvin, P. R., Why Kinesin Is So Processive. *Proc. Natl. Acad. Sci. U. S. A.* **2009,** *106* (31), 12717-22.
2. Visscher, K.; Schnitzer, M. J.; Block, S. M., Single Kinesin Molecules Studied with a Molecular Force Clamp. *Nature* **1999,** *400* (6740), 184-9.
3. Berg, H. C., Bacterial Flagellar Motor. *Current biology : CB* **2008,** *18* (16), R689-91.
4. Noji, H.; Yasuda, R.; Yoshida, M.; Kinosita, K., Direct Observation of the Rotation of F-1-Atpase. *Nature* **1997,** *386* (6622), 299-302.
5. Enoki, S.; Iino, R.; Niitani, Y.; Minagawa, Y.; Tomishige, M.; Noji, H., High-Speed Angle-Resolved Imaging of a Single Gold Nanorod with Microsecond Temporal Resolution and One-Degree Angle Precision. *Anal Chem* **2015,** *87* (4), 2079-86.
6. Martin, J. L.; Ishmukhametov, R.; Hornung, T.; Ahmad, Z.; Frasch, W. D., Anatomy of F1-Atpase Powered Rotation. *Proc Natl Acad Sci U S A* **2014,** *111* (10), 3715-20.
7. Bath, J.; Green, S. J.; Turberfield, A. J., A Free-Running DNA Motor Powered by a Nicking Enzyme. *Angewandte Chemie* **2005,** *117* (28), 4432-4435.
8. Mai, J.; Sokolov, I. M.; Blumen, A., Directed Particle Diffusion under "Burnt Bridges" Conditions. *Physical review. E, Statistical, nonlinear, and soft matter physics* **2001,** *64* (1 Pt 1), 011102.
9. Collins, B. S. L.; Kistemaker, J. C. M.; Otten, E.; Feringa, B. L., A Chemically Powered Unidirectional Rotary Molecular Motor Based on a Palladium Redox Cycle. *Nat. Chem.* **2016,** *8* (9), 860-866.
10. Kay, E. R.; Leigh, D. A.; Zerbetto, F., Synthetic Molecular Motors and Mechanical Machines. *Angew. Chem. Int. Ed. Engl.* **2007,** *46* (1-2), 72-191.
11. Erbas-Cakmak, S.; Leigh, D. A.; McTernan, C. T.; Nussbaumer, A. L., Artificial Molecular Machines. *Chemical reviews* **2015,** *115* (18), 10081-10206.
12. Pan, J.; Li, F.; Cha, T.; Chen, H.; Choi, J. H., Recent Progress on DNA Based Walkers. *Current opinion in biotechnology* **2014,** *34C*, 56-64.
13. Abendroth, J. M.; Bushuyev, O. S.; Weiss, P. S.; Barrett, C. J., Controlling Motion at the Nanoscale: Rise of the Molecular Machines. *ACS Nano* **2015,** *9* (8), 7746-7768.
14. Kinbara, K.; Aida, T., Toward Intelligent Molecular Machines: Directed Motions of Biological and Artificial Molecules and Assemblies. *Chemical reviews* **2005,** *105* (4), 1377-1400.
15. Huang, T. J.; Juluri, B. K., Biological and Biomimetic Molecular Machines. *Nanomedicine-Uk* **2008,** *3* (1), 107-124.
16. Fletcher, S. P.; Dumur, F.; Pollard, M. M.; Feringa, B. L., A Reversible, Unidirectional Molecular Rotary Motor Driven by Chemical Energy. *Science* **2005,** *310* (5745), 80-82.
17. Wilson, M. R.; Solà, J.; Carlone, A.; Goldup, S. M.; Lebrasseur, N.; Leigh, D. A., An Autonomous Chemically Fuelled Small-Molecule Motor. *Nature* **2016,** *534* (7606), 235-240.
18. You, M. X.; Huang, F. J.; Chen, Z.; Wang, R. W.; Tan, W. H., Building a Nanostructure with Reversible Motions Using Photonic Energy. *ACS Nano* **2012,** *6* (9), 7935-7941.
19. Koumura, N.; Zijlstra, R. W. J.; van Delden, R. A.; Harada, N.; Feringa, B. L., Light-Driven Monodirectional Molecular Rotor. *Nature* **1999,** *401* (6749), 152-155.

20. Kudernac, T.; Ruangsupapichat, N.; Parschau, M.; Maciá, B.; Katsonis, N.; Harutyunyan, S. R.; Ernst, K.-H.; Feringa, B. L., Electrically Driven Directional Motion of a Four-Wheeled Molecule on a Metal Surface. *Nature* **2011,** *479* (7372), 208-211.

21. Maier, A. M.; Weig, C.; Oswald, P.; Frey, E.; Fischer, P.; Liedl, T., Magnetic Propulsion of Microswimmers with DNA-Based Flagellar Bundles. *Nano letters* **2016,** *16* (2), 906-910.

22. Gennerich, A.; Vale, R. D., Walking the Walk: How Kinesin and Dynein Coordinate Their Steps. *Current opinion in cell biology* **2009,** *21* (1), 59-67.

23. Simmel, F. C., Processive Motion of Bipedal DNA Walkers. *ChemPhysChem* **2009,** *10* (15), 2593-7.

24. Seeman, N. C., From Genes to Machines: DNA Nanomechanical Devices. *Trends Biochem.Sci.* **2005,** *30* (3), 119-125.

25. Krishnan, Y.; Simmel, F. C., Nucleic Acid Based Molecular Devices. *Angew. Chem. Int. Ed. Engl.* **2011,** *50* (14), 3124-3156.

26. Green, S. J.; Bath, J.; Turberfield, A. J., Coordinated Chemomechanical Cycles: A Mechanism for Autonomous Molecular Motion. *Physical Review Letters* **2008,** *101* (23).

27. Bath, J.; Green, S. J.; Allen, K. E.; Turberfield, A. J., Mechanism for a Directional, Processive, and Reversible DNA Motor. *Small* **2009,** *5* (13), 1513-1516.

28. Seeman, N. C., Nanomaterials Based on DNA. *Annu Rev Biochem* **2010,** *79*, 65-87.

29. Jones, M. R.; Seeman, N. C.; Mirkin, C. A., Nanomaterials. Programmable Materials and the Nature of the DNA Bond. *Science* **2015,** *347* (6224), 1260901.

30. Rothemund, P. W., Folding DNA to Create Nanoscale Shapes and Patterns. *Nature* **2006,** *440* (7082), 297-302.

31. Douglas, S. M.; Dietz, H.; Liedl, T.; Hogberg, B.; Graf, F.; Shih, W. M., Self-Assembly of DNA into Nanoscale Three-Dimensional Shapes. *Nature* **2009,** *459* (7245), 414-418.

32. Ke, Y.; Voigt, N. V.; Gothelf, K. V.; Shih, W. M., Multilayer DNA Origami Packed on Hexagonal and Hybrid Lattices. *J. Am. Chem. Soc.* **2012,** *134* (3), 1770-4.

33. Jungmann, R.; Scheible, M.; Kuzyk, A.; Pardatscher, G.; Castro, C. E.; Simmel, F. C., DNA Origami-Based Nanoribbons: Assembly, Length Distribution, and Twist. *Nanotechnology* **2011,** *22* (27).

34. Liu, W.; Zhong, H.; Wang, R.; Seeman, N. C., Crystalline Two-Dimensional DNA-Origami Arrays. *Angew. Chem. Int. Ed. Engl.* **2011,** *50* (1), 264-7.

35. Rajendran, A.; Endo, M.; Katsuda, Y.; Hidaka, K.; Sugiyama, H., Programmed Two-Dimensional Self-Assembly of Multiple DNA Origami Jigsaw Pieces. *ACS Nano* **2011,** *5* (1), 665-71.

36. Li, Z.; Liu, M.; Wang, L.; Nangreave, J.; Yan, H.; Liu, Y., Molecular Behavior of DNA Origami in Higher-Order Self-Assembly. *J. Am. Chem. Soc.* **2010,** *132* (38), 13545-52.

37. Gerling, T.; Wagenbauer, K. F.; Neuner, A. M.; Dietz, H., Dynamic DNA Devices and Assemblies Formed by Shape-Complementary, Non-Base Pairing 3d Components. *Science* **2015,** *347* (6229), 1446-52.

38. Liber, M.; Tomov, T. E.; Tsukanov, R.; Berger, Y.; Nir, E., A Bipedal DNA Motor That Travels Back and Forth between Two DNA Origami Tiles. *Small* **2015,** *11* (5), 568-75.

39. Wickham, S. F.; Endo, M.; Katsuda, Y.; Hidaka, K.; Bath, J.; Sugiyama, H.; Turberfield, A. J., Direct Observation of Stepwise Movement of a Synthetic Molecular Transporter. *Nat. Nanotechnol.* **2011,** *6* (3), 166-9.

40. Wickham, S. F.; Bath, J.; Katsuda, Y.; Endo, M.; Hidaka, K.; Sugiyama, H.; Turberfield, A. J., A DNA-Based Molecular Motor That Can Navigate a Network of Tracks. *Nat. Nanotechnol.* **2012,** *7* (3), 169-73.

41. Lund, K.; Manzo, A. J.; Dabby, N.; Michelotti, N.; Johnson-Buck, A.; Nangreave, J.; Taylor, S.; Pei, R. J.; Stojanovic, M. N.; Walter, N. G., et al., Molecular Robots Guided by Prescriptive Landscapes. *Nature* **2010,** *465* (7295), 206-210.

42. Gu, H. Z.; Chao, J.; Xiao, S. J.; Seeman, N. C., A Proximity-Based Programmable DNA Nanoscale Assembly Line. *Nature* **2010,** *465* (7295), 202-205.

43. Zhou, C.; Duan, X.; Liu, N., A Plasmonic Nanorod That Walks on DNA Origami. *Nat Commun* **2015,** *6*, 8102.

44. Tomov, T. E.; Tsukanov, R.; Liber, M.; Masoud, R.; Plavner, N.; Nir, E., Rational Design of DNA Motors: Fuel Optimization through Single-Molecule Fluorescence. *J Am Chem Soc* **2013,** *135* (32), 11935-41.

45. Urban, M. J.; Zhou, C.; Duan, X.; Liu, N., Optically Resolving the Dynamic Walking of a Plasmonic Walker Couple. *Nano letters* **2015,** *15* (12), 8392-8396.

46. Yurke, B.; Turberfield, A. J.; Mills, A. P.; Simmel, F. C.; Neumann, J. L., A DNA-Fuelled Molecular Machine Made of DNA. *Nature* **2000,** *406* (6796), 605-608.

47. Sherman, W. B.; Seeman, N. C., A Precisely Controlled DNA Biped Walking Device. *Nano Lett.* **2004,** *4* (7), 1203-1207.

48. Shin, J. S.; Pierce, N. A., A Synthetic DNA Walker for Molecular Transport. *J Am Chem Soc* **2004,** *126* (35), 10834-5.

49. Yin, P.; Yan, H.; Daniell, X. G.; Turberfield, A. J.; Reif, J. H., A Unidirectional DNA Walker That Moves Autonomously Along a Track. *Angew. Chem. Int. Ed. Engl.* **2004,** *43* (37), 4906-4911.

50. Tian, Y.; Mao, C. D., Molecular Gears: A Pair of DNA Circles Continuously Rolls against Each Other. *J. Am. Chem. Soc.* **2004,** *126* (37), 11410-11411.

51. Yin, P.; Choi, H. M. T.; Calvert, C. R.; Pierce, N. A., Programming Biomolecular Self-Assembly Pathways. *Nature* **2008,** *451* (7176), 318-U4.

52. Omabegho, T.; Sha, R.; Seeman, N. C., A Bipedal DNA Brownian Motor with Coordinated Legs. *Science* **2009,** *324* (5923), 67-71.

53. Muscat, R. A.; Bath, J.; Turberfield, A. J., A Programmable Molecular Robot. *Nano Lett.* **2011,** *11* (3), 982-7.

54. Masoud, R.; Tsukanov, R.; Tomov, T. E.; Plavner, N.; Liber, M.; Nir, E., Studying the Structural Dynamics of Bipedal DNA Motors with Single-Molecule Fluorescence Spectroscopy. *ACS Nano* **2012,** *6* (7), 6272-83.

55. Green, S. J.; Lubrich, D.; Turberfield, A. J., DNA Hairpins: Fuel for Autonomous DNA Devices. *Biophys. J.* **2006,** *91* (8), 2966-75.

56. Marras, A. E.; Zhou, L.; Su, H. J.; Castro, C. E., Programmable Motion of DNA Origami Mechanisms. *Proc Natl Acad Sci U S A* **2015,** *112* (3), 713-8.

57. Zhou, L.; Marras, A. E.; Su, H. J.; Castro, C. E., Direct Design of an Energy Landscape with Bistable DNA Origami Mechanisms. *Nano letters* **2015,** *15* (3), 1815-21.

58. Sobczak, J. P.; Martin, T. G.; Gerling, T.; Dietz, H., Rapid Folding of DNA into Nanoscale Shapes at Constant Temperature. *Science* **2012,** *338* (6113), 1458-61.

59. Funke, J. J.; Dietz, H., Placing Molecules with Bohr Radius Resolution Using DNA Origami. *Nature nanotechnology* **2016,** *11* (1), 47-52.

60. Douglas, S. M.; Bachelet, I.; Church, G. M., A Logic-Gated Nanorobot for Targeted Transport of Molecular Payloads. *Science* **2012,** *335* (6070), 831-834.

61. Ketterer, P.; Willner, E. M.; Dietz, H., Nanoscale Rotary Apparatus Formed from Tight-Fitting 3d DNA Components. *Science advances* **2016,** *2* (2), e1501209.

62. Glick, Y.; Avrahami, D.; Michaely, E.; Gerber, D., High-Throughput Protein Expression Generator Using a Microfluidic Platform. *Journal of visualized experiments : JoVE* **2012,** (66), e3849.

63. Thorsen, T.; Maerkl, S. J.; Quake, S. R., Microfluidic Large-Scale Integration. *Science* **2002,** *298* (5593), 580-4.

64. Tsukanov, R.; Tomov, T. E.; Liber, M.; Berger, Y.; Nir, E., Developing DNA Nanotechnology Using Single-Molecule Fluorescence. *Acc Chem Res* **2014,** *47* (6), 1789-98.

65. Tsukanov, R.; Tomov, T. E.; Masoud, R.; Drory, H.; Plavner, N.; Liber, M.; Nir, E., Detailed Study of DNA Hairpin Dynamics Using Single-Molecule Fluorescence Assisted by DNA Origami. *J Phys Chem B* **2013,** *117* (40), 11932-42.

66. He, Y.; Liu, D. R., Autonomous Multistep Organic Synthesis in a Single Isothermal Solution Mediated by a DNA Walker. *Nat. Nanotechnol.* **2010,** *5* (11), 778-782.

67. List, J.; Falgenhauer, E.; Kopperger, E.; Pardatscher, G.; Simmel, F. C., Long-Range Movement of Large Mechanically Interlocked DNA Nanostructures. *Nat. Commun.* **2016,** *7*, 12414.

68. Nickels, P. C.; Wünsch, B.; Holzmeister, P.; Bae, W.; Kneer, L. M.; Grohmann, D.; Tinnefeld, P.; Liedl, T., Molecular Force Spectroscopy with a DNA Origami–Based Nanoscopic Force Clamp. *Science* **2016,** *354* (6310), 305-307.

69. Le, J. V.; Luo, Y.; Darcy, M. A.; Lucas, C. R.; Goodwin, M. F.; Poirier, M. G.; Castro, C. E., Probing Nucleosome Stability with a DNA Origami Nanocaliper. *ACS Nano* **2016,** *10* (7), 7073-7084.

70. Seelig, G.; Soloveichik, D.; Zhang, D. Y.; Winfree, E., Enzyme-Free Nucleic Acid Logic Circuits. *Science* **2006,** *314* (5805), 1585-8.

71. Qian, L. L.; Winfree, E., Scaling up Digital Circuit Computation with DNA Strand Displacement Cascades. *Science* **2011,** *332* (6034), 1196-1201.

72. Boemo, M. A.; Lucas, A. E.; Turberfield, A. J.; Cardelli, L., The Formal Language and Design Principles of Autonomous DNA Walker Circuits. *ACS Synthetic Biology* **2016,** *5* (8), 878-884.

73. Jungmann, R.; Steinhauer, C.; Scheible, M.; Kuzyk, A.; Tinnefeld, P.; Simmel, F. C., Single-Molecule Kinetics and Super-Resolution Microscopy by Fluorescence Imaging of Transient Binding on DNA Origami. *Nano Lett.* **2010,** *10* (11), 4756-61.

74. Douglas, S. M.; Marblestone, A. H.; Teerapittayanon, S.; Vazquez, A.; Church, G. M.; Shih, W. M., Rapid Prototyping of 3d DNA-Origami Shapes with Cadnano. *Nucleic Acids Res.* **2009,** *37* (15), 5001-5006.

75. Kim, D. N.; Kilchherr, F.; Dietz, H.; Bathe, M., Quantitative Prediction of 3d Solution Shape and Flexibility of Nucleic Acid Nanostructures. *Nucleic Acids Res.* **2012,** *40* (7), 2862-2868.

76. Stahl, E.; Martin, T. G.; Praetorius, F.; Dietz, H., Facile and Scalable Preparation of Pure and Dense DNA Origami Solutions. *Angew Chem Int Ed Engl* **2014,** *53* (47), 12735-40.

77. Tang, G.; Peng, L.; Baldwin, P. R.; Mann, D. S.; Jiang, W.; Rees, I.; Ludtke, S. J., Eman2: An Extensible Image Processing Suite for Electron Microscopy. *J Struct Biol* **2007,** *157* (1), 38-46.

78. Scheres, S. H. W.; Nunez-Ramirez, R.; Sorzano, C. O. S.; Carazo, J. M.; Marabini, R., Image Processing for Electron Microscopy Single-Particle Analysis Using Xmipp. *Nature protocols* **2008,** *3* (6), 977-990.

79. Krishnan, S.; Ziegler, D.; Arnaut, V.; Martin, T. G.; Kapsner, K.; Henneberg, K.; Bausch, A. R.; Dietz, H.; Simmel, F. C., Molecular Transport through Large-Diameter DNA Nanopores. *Nat. Commun.* **2016,** *7*, 12787.

80. Marras, A. E.; Zhou, L.; Kolliopoulos, V.; Su, H. J.; Castro, C. E., Directing Folding Pathways for Multi-Component DNA Origami Nanostructures with Complex Topology. *New Journal of Physics* **2016,** *18* (5), 055005.

81. Tomov, T. E.; Tsukanov, R.; Masoud, R.; Liber, M.; Plavner, N.; Nir, E., Disentangling Subpopulations in Single-Molecule Fret and Alex Experiments with Photon Distribution Analysis. *Biophys. J.* **2012,** *102* (5), 1163-73.

82. Zhao, Z.; Yan, H.; Liu, Y., A Route to Scale up DNA Origami Using DNA Tiles as Folding Staples. *Angewandte Chemie International Edition* **2010,** *49* (8), 1414-1417.

83. Pal, S.; Deng, Z.; Wang, H.; Zou, S.; Liu, Y.; Yan, H., DNA Directed Self-Assembly of Anisotropic Plasmonic Nanostructures. *J Am Chem Soc* **2011,** *133* (44), 17606-9.

84. Vietz, C.; Lalkens, B.; Acuna, G. P.; Tinnefeld, P., Functionalizing Large Nanoparticles for Small Gaps in Dimer Nanoantennas. *New Journal of Physics* **2016,** *18* (4), 045012.

85. Acuna, G. P.; Moller, F. M.; Holzmeister, P.; Beater, S.; Lalkens, B.; Tinnefeld, P., Fluorescence Enhancement at Docking Sites of DNA-Directed Self-Assembled Nanoantennas. *Science* **2012,** *338* (6106), 506-10.

86. Kuzyk, A.; Schreiber, R.; Fan, Z.; Pardatscher, G.; Roller, E.-M.; Högele, A.; Simmel, F. C.; Govorov, A. O.; Liedl, T., DNA-Based Self-Assembly of Chiral Plasmonic Nanostructures with Tailored Optical Response. *Nature* **2012,** *483* (7389), 311-314.

87. Karedla, N.; Stein, S. C.; Hahnel, D.; Gregor, I.; Chizhik, A.; Enderlein, J., Simultaneous Measurement of the Three-Dimensional Orientation of Excitation and Emission Dipoles. *Phys Rev Lett* **2015,** *115* (17), 173002.

88. Patra, D.; Gregor, I.; Enderlein, J., Image Analysis of Defocused Single-Molecule Images for Three-Dimensional Molecule Orientation Studies. *J. Phys. Chem. A* **2004,** *108* (33), 6836-6841.